Sawala, T, Frenk, CS, Fattahi, A, Navarro, JF, Theuns, T, Bower, RG, Crain, RA, Furlong, M, Jenkins, A, Schaller, M and Schaye, J

 The chosen few: the low mass halos that host faint galaxies

http://researchonline.ljmu.ac.uk/id/eprint/916/

Article

The chosen few: the low-mass haloes that host faint galaxies

Till Sawala,[1]★ Carlos S. Frenk,[1] Azadeh Fattahi,[2] Julio F. Navarro,[2] Tom Theuns,[1] Richard G. Bower,[1] Robert A. Crain,[3,4] Michelle Furlong,[1] Adrian Jenkins,[1] Matthieu Schaller[1] and Joop Schaye[3]

[1]*Institute for Computational Cosmology, Department of Physics, University of Durham, South Road, Durham DH13LE, UK*
[2]*Department of Physics and Astronomy, University of Victoria, 3800 Finnerty Road, Victoria, BC V8P 5C2, Canada*
[3]*Leiden Observatory, Leiden University, Postbus 9513, NL-2300 RA Leiden, the Netherlands*
[4]*Astrophysics Research Institute, Liverpool John Moores University, 146 Brownlow Hill, Liverpool L3 5RF, UK*

ABSTRACT

Since reionization prevents star formation in most haloes less massive than $3 \times 10^9\,\mathrm{M}_\odot$, dwarf galaxies only populate a fraction of existing dark matter haloes. We use hydrodynamic cosmological simulations of the Local Group to study the discriminating factors for galaxy formation in the early Universe and connect them to the present-day properties of galaxies and haloes. A combination of selection effects related to reionization, and the subsequent evolution of haloes in different environments, introduces strong biases between the population of haloes that host dwarf galaxies, and the total halo population. Haloes that host galaxies formed earlier and are more concentrated. In addition, haloes more affected by tidal stripping are more likely to host a galaxy for a given mass or maximum circular velocity, $v_{\max}$, today. Consequently, satellite haloes are populated more frequently than field haloes, and satellite haloes of 10^8–$10^9\,\mathrm{M}_\odot$ or $v_{\max}$ of 12–20 km s^{-1}, compatible with stellar kinematics of Local Group dwarf spheroidals, have experienced a greater than average reduction in both mass and $v_{\max}$ after infall. They are on closer, more radial orbits with higher infall velocities and earlier infall times. Together, these effects make dwarf galaxies highly biased tracers of the underlying dark matter distribution.

Key words: methods: numerical – galaxies: dwarf – galaxies: formation – Local Group – cosmology: theory.

There are some who are in darkness
And the others are in light
And you see the ones in brightness
Those in darkness drop from sight
– Bertolt Brecht, *The Threepenny Opera*

1 INTRODUCTION

The Local Group dwarf galaxies and their haloes are often described as ideal test cases for the impact of cosmological models on small-scale structures. It has, of course, long been recognized that astrophysical processes such as reionization can suppress star formation in low-mass haloes (e.g. Efstathiou 1992; Bullock, Kravtsov & Weinberg 2000; Benson et al. 2002; Somerville 2002). It should therefore perhaps come as no surprise that the total number of substructures predicted in a given cosmological model can be far greater than the number of observable galaxies. However, as reionization occurs in the early universe when haloes are at a fraction of their

final mass, it is also expected that the properties of Local Group haloes and galaxies today are only loosely related to the conditions which separated those progenitor haloes that were able to form stars from those that have remained dark.

In this paper, we examine how the sparse sampling of haloes by galaxies in the presence of an ionizing background, and the subsequent evolution of haloes and galaxies in a Local Group environment, can lead to a population of haloes hosting faint galaxies that is very different from the total halo population.

Previous simulations have studied the impact of reionization both for individual dwarf galaxies and for satellites of Milky Way sized haloes. Okamoto, Gao & Theuns (2008) and Okamoto & Frenk (2009) have found that reionization can remove most of the baryons from haloes with low maximum circular velocity, $v_{\max}$ (the circular velocity measured at the radius where $v_{\mathrm{circ}} = \sqrt{GM(< \mathrm{r})/\mathrm{r}}$ is maximal), and showed that dark satellite haloes are expected around the Milky Way with $v_{\max}$ up to 25 km s^{-1}. They concluded that $v_{\max} \sim 12$ km s^{-1} at the time of reionization ($z = 8$ in their model) sharply separates dark and luminous haloes. Nickerson et al. (2011) have also performed a simulation of a Milky Way mass halo and its satellites, but found the peak mass, M_{peak}, which satellites reach

★ E-mail: till.sawala@durham.ac.uk

during their evolution to be the discriminating factor, with haloes of $M_{peak} < 2 \times 10^9 \, M_\odot$ losing most of their gas to reionization and failing to form stars. Shen et al. (2014) simulated galaxy formation in seven haloes of mass between 4.4×10^8 and $3.6 \times 10^{10} \, M_\odot$, and found that the three haloes with a peak value of $v_{max} < 16$ km s^{-1} were devoid of stars, and two haloes with peak mass of 1.8 and $3.3 \times 10^9 \, M_\odot$ only started star formation at $z \sim 0.5$, long after reionization.

Recently, we used a set of cosmological hydrodynamic simulations of Local Group like volumes to show that the appearance of 'dark' haloes that host no galaxy, combined with the reduction in halo mass due to baryonic processes, can significantly change the expected stellar-to-total mass relation of dwarf galaxies, and resolve previously reported discrepancies between observations of individual dwarf galaxies and the predictions of ΛCDM derived from abundance matching (Sawala et al. 2015, see also Sawala et al. 2011). In this paper, we use the same set of simulations to study how reionization selects between haloes that host galaxies and those that do not. Following the formation and evolution of dark and luminous haloes throughout cosmic time, we can connect their properties in the early universe to the observable galaxies and haloes of the present day.

We also link individual haloes from the hydrodynamic simulations to their counterparts in dark matter only (DMO) simulations of the same volumes. This allows us to study the intrinsic properties of haloes which determine galaxy formation, and distinguish them from the impact that the baryonic processes associated with galaxy formation can have on individual haloes. Finally, by comparing the populations of dark and luminous haloes in the simulated Local Group volumes, we deduce the biases which can arise when observed galaxies are assumed to be representative of the underlying population of dark matter haloes.

This paper is organized as follows. In Section 2, we briefly describe the simulations and the astrophysical assumptions made. By comparing simulations with and without reionization, we discuss the impact of reionization in Section 3. Section 4 describes galaxy formation in the presence of reionization. In Section 4.1, we explain how the assembly histories separate those haloes which form stars from those that remain dark. We discuss trends in the star formation times in Section 4.2. In Section 4.3 we discuss the resulting bias in formation redshifts, and in Section 4.4 we show the difference in concentration between luminous and non-luminous haloes. In Section 5, we examine how the subsequent evolution in different environments within the Local Group creates further biases between luminous and non-luminous haloes: satellites haloes that are luminous have higher infall redshifts and more radial orbits with higher infall velocities (Section 5.1), and the distributions of luminous and non-luminous haloes differ within the Local Group (Section 5.2). We discuss some implications of our findings and conclude with a summary in Section 6.

2 METHODS

The simulations used in this paper have previously been described in Sawala et al. (2014, 2015). We reproduce here the main aspects of their initial conditions and astrophysical model.

We resimulate 12 cosmological volumes as 'zoom' simulations extracted frome the DOVE simulation, a $100^3 \, Mpc^3$ *N*-Body simulation based on the *WMAP*-7 cosmology. We require that each volume should contain two haloes of mass in the range $(5 \times 10^{11}$–$2.5 \times 10^{12}) \, M_\odot$ separated by 800 ± 200 kpc, approaching with radial velocity of $(0$–$250)$ km s^{-1} and with tangential velocity be-

Table 1. Numerical parameters of the simulations.

| Label | Type | Particle masses | | Max softening |
		DM ($M_\odot$)	Gas ($M_\odot$)	(pc/h)
L1	hydro	5.0×10^4	1.0×10^4	94
L1	DMO	6.0×10^4	–	94
L2	hydro	5.9×10^5	1.3×10^5	216
L2	DMO	7.2×10^5	–	216
L3	hydro	7.3×10^6	1.5×10^6	500
L3	DMO	8.8×10^6	–	500

low 100 km s^{-1} in an environment with an unperturbed Hubble flow out to 4 Mpc. The high-resolution initial conditions were created using second-order Lagrangian perturbation theory, as described by Jenkins (2010). The selection of Local Group environments is discussed in more detail in Fattahi et al. (2015). The simulations were performed using a pressure-entropy variant (Hopkins 2013) of the Tree-PM SPH code P-GADGET3 (Springel 2005), described in Schaller et al. (2015). The subgrid physics model is that of the *Evolution and Assembly of GaLaxies and their Environments* project (EAGLE), described by Schaye et al. (2015) and Crain et al. (2015). It includes metal-dependent radiative cooling (Wiersma, Schaye & Smith 2009a) and photoheating in the presence of UV and X-ray backgrounds, and the cosmic microwave background (CMB).

Prior to reionization, net cooling rates are computed from the CMB and from a UV and X-ray background that follows the $z = 9$ model of Haardt & Madau (2001) with a 1 Ryd high-energy cut-off. To account for the temperature boost due to radiative transfer and non-equilibrium effects over the optically thin limit assumed in our simulations (Abel & Haehnelt 1999), we inject 2 eV per hydrogen and helium atom. We assume that hydrogen reionizes instantaneously at $z = 11.5$ (Planck Collaboration XVI 2014), while the redshift dependence of helium reionization is modelled as a Gaussian centred at $z = 3.5$ (Theuns et al. 2002) with $\sigma(z) = 0.5$. As shown by Wiersma et al. (2009b) and Rollinde et al. (2013), the resulting evolution of the temperature–density relation is consistent with measurements of the intergalactic medium (Schaye et al. 2000).

Star formation follows the formulation of Schaye & Dalla Vecchia (2008) with a metallicity-dependent threshold (Schaye 2004). The model includes stellar evolution (Wiersma et al. 2009b) and stochastic thermal supernova feedback (Dalla Vecchia & Schaye 2012), as well as black hole growth and AGN feedback (Springel, Di Matteo & Hernquist 2005; Booth & Schaye 2009; Rosas-Guevara et al. 2015).

All simulations were run twice: once with gas and the baryon physics described above, and once as DMO. In addition, one volume was also run with the complete hydrodynamic model, but without reionization. In the DMO simulations the dark matter particle masses are larger by a factor of $(\Omega_b + \Omega_{DM})/\Omega_{DM}$ relative to the corresponding hydrodynamic simulations. To investigate the regime of Local Group dwarf galaxies, we use three different resolution levels labelled L1, L2 and L3, whose parameters are given in Table 1. In this work, L3 is only used to test convergence. The main results for the model that includes reionization are obtained from 12 pairs of hydrodynamic and DMO simulations at resolution L2 and one pair at L1. The simulations without reionization presented in Section 3 were only run up to L2.

We use a Friends-of-Friends algorithm (FoF; Davis et al. 1985) to identify overdense structures (FoF-groups), and the SUBFIND algorithm (Springel et al. 2001; Dolag et al. 2009) to identify self-bound substructures within them. As they represent the objects

most directly associated with individual galaxies, we always refer to the self-bound substructures as 'haloes'. The principal substructure within an FoF-group contains most of its mass, but satellites may share the same FoF-group while still residing in separate self-bound haloes.

Throughout this paper, we use the term 'satellite' when we refer to the satellite haloes or galaxies associated with the M31 and Milky Way analogues, and 'field' when we refer to isolated haloes. Haloes containing at least one star particle at $z = 0$ will be called 'luminous', while others will be called 'dark' or 'non-luminous'. Although the stellar mass limit depends on resolution, as discussed in Section 3, when we include reionization the number of luminous haloes is converged.

We analyse our simulations at 128 snapshots, and trace the evolution of individual haloes in both the hydrodynamic and DMO simulations using merger trees, as described by Helly et al. ([2003](#)) and Jiang et al. ([2014](#)). The unique IDs of dark matter particles which encode their positions in the initial conditions allow us to match and compare individual haloes from different simulations of the same volume at the same resolution.

3 THE IMPACT OF REIONIZATION

From $z = 11.5$, the UV background heats the intergalactic medium and lowers its cooling rate. It can also remove gas from low-mass haloes by photoevaporation. In Fig. [1](#), we compare the evolution of the gas density distributions in two simulations of the same volume and resolution (L2) with and without reionization, as well as the final stellar density distribution. At $z = 10$, shortly after hydrogen reionization, the main difference is apparent in the low-density regions. Here, the thermal energy provided by reionization slows the collapse of small structures which results in a smoother intergalactic medium (IGM) than in the absence of reionization. By comparison, regions of higher density which correspond to haloes that have already formed before reionization, are not significantly affected. By $z = 4$, the intergalactic medium has become significantly more fragmented in the simulation without reionization, with many more low-mass haloes now containing dense gas and forming stars compared to the simulation with reionization. At $z = 0$, it can be seen that while the large-scale features in both the gas- and stellar density distributions are similar, in the absence of reionization, the IGM is strongly fragmented and has collapsed into many small clumps. By contrast, the IGM in the simulation with reionization has remained much smoother. Without reionization, the number of haloes within 2.5 Mpc from the LG centre that contain stars is ∼700, compared to only ∼180 in the same volume with reionization.

In Fig. [2](#) we compare the fraction of haloes containing stars at $z = 0$, for simulations of the same volume with and without reionization and at different resolutions, as defined in Table [1](#). It can be seen that significantly more haloes are luminous in the simulations without reionization. It should be noted that our simulations are not sufficient to simulate a Universe without reionization faithfully: the level of fragmentation of the IGM is limited by resolution, and the total number of galaxies formed in this (unphysical) scenario is not converged and increases with increasing resolution. By contrast, the results with reionization are well converged at L2, suggesting that in our simulations, reionization sets a limit for star formation in low-mass haloes that is above the resolution limit of our simulations.

Fig. [3](#) shows the evolution of the luminous fraction of haloes as a function of mass in a simulation that includes reionization, from $z = 11.5$ to $z0$. At all redshifts, the fraction of luminous haloes at 10^8 M$_\odot$ is less than 10 per cent, and almost no haloes are

luminous below $10^{7.5}$ M$_\odot$. The mass dependence of the luminous fraction is strongest at $z = 11.5$, where all haloes more massive than 3×10^8 M$_\odot$ contain stars. As haloes typically grow in mass over time, the mass dependence of the luminous fraction becomes more gradual towards lower redshifts. While the minimum halo mass of luminous haloes remains almost unchanged, the mass at which most haloes are luminous increases continuously.

Of course, supernovae and AGN feedback can also heat up the gas and regulate star formation in larger haloes. However, reionization is clearly a key factor for determining the total number of galaxies thats form and can also strengthen the impact of supernovae on the star formation rate (Pawlik & Schaye [2009](#)). In terms of the halo properties required for star formation in the presence of reionization, our results are consistent with those obtained by the previous studies reviewed in Section 1. At a mass of $\sim 3 \times 10^9$ M$_\odot$, or $v_{max} \sim 25$ km s^{-1}, half of all haloes contain galaxies at $z = 0$. Based on the measured stellar-halo mass relation inferred from observations and reproduced in our simulations (Sawala et al. [2014](#), [2015](#)), we therefore expect the selection effects described here to be significant for galaxies up to $M_\star \sim 10^{6.5}$ M$_\odot$ or $M_v \sim -12$, including most dwarf spheroidals and fainter dwarf irregulars (Weisz et al. [2014a](#)).

4 THE TIMING OF GALAXY FORMATION

Since reionization takes place at a time when haloes have only a small fraction of their present mass, the probability for star formation within a halo is expected to depend strongly on its individual assembly history. Consequently, the properties that separate the haloes that host galaxies from those that remain dark should be more closely related to their progenitors at high redshifts.

Haloes that have assembled more mass at the time of reionization will be more resilient to photoevaporation, and will subsequently be able to cool gas more efficiently, resulting in a greater chance for star formation. As a result, for a fixed mass today, haloes that formed earlier are more likely to contain galaxies, so that haloes that host galaxies are biased towards earlier formation times.

4.1 Assembly histories

In Fig. [4](#) we compare the average mass assembly histories of luminous and dark haloes in three different final halo mass ranges. We distinguish between presently isolated haloes and satellites, and compare the results measured directly in the hydrodynamic simulation to those measured by comparing the matched counterparts to the luminous and non-luminous haloes from the DMO simulation.

As expected, we find that haloes which form stars assemble their mass significantly earlier compared to non-luminous haloes of the same mass today.

We reproduce the well-known result of hierarchical structure formation that haloes of lower mass typically form earlier than haloes of larger mass, independently of whether or not they contain stars. Because most haloes above $10^{9.5}$ M$_\odot$ are luminous, we find only a slight difference between the assembly histories of dark and luminous haloes above this mass. However, as the fraction of luminous haloes decreases in the mass ranges 10^9–$10^{9.5}$ M$_\odot$ and $10^{8.5}$–10^9 M$_\odot$, the remaining luminous haloes are increasingly biased towards earlier mass assembly. This result can be readily understood from the fact that for gas cooling and star formation to take place in the presence of reionization, a sufficiently high mass needs to have been assembled at an early time.

As shown in the middle column of Fig. [4](#), luminous as well as dark satellites of all masses have typically experienced some degree
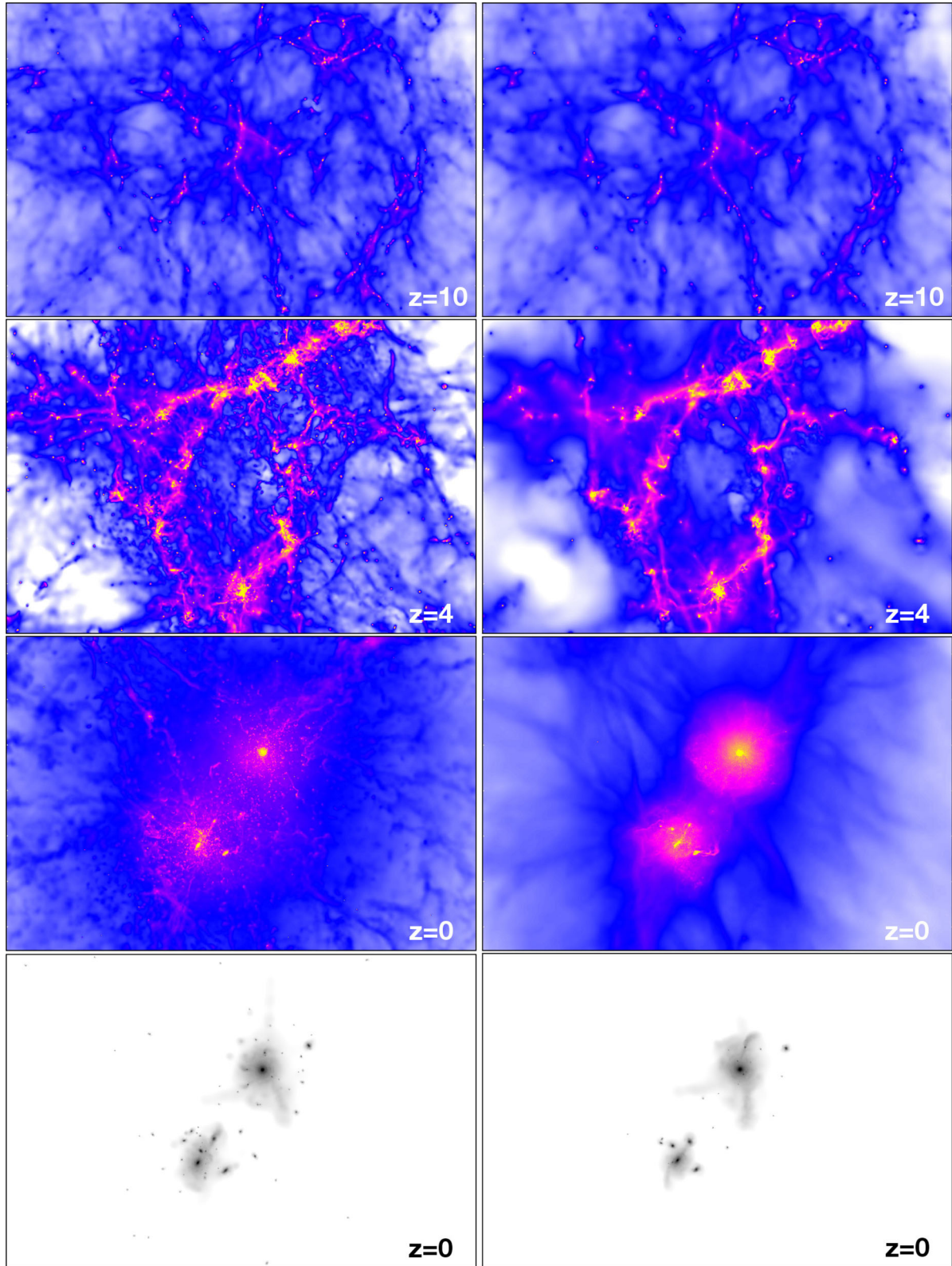
Figure 1. Gas density distribution (top three rows) and stellar density distribution (bottom row, only haloes with $m_\star > 4 \times 10^6 \, \mathrm{M}_\odot$) in the L2 simulation without reionization (left) and the same volume with reionization (right). The region shown measures $3 \times 2 \, \mathrm{Mpc}^2$ at $z = 0$ and is magnified proportional to $a(z)$ at higher redshifts. Following reionization at $z = 11.5$, gas is removed from low-mass haloes, and reduced cooling results in a less fragmented IGM. The impact of reionization is first noticeable in the low-density regions, which are already less structured at $z = 10$, just after reionization. At later times, the differences increase, and the number of collapsed and eventually star-forming haloes is much lower in the simulation that includes reionization.
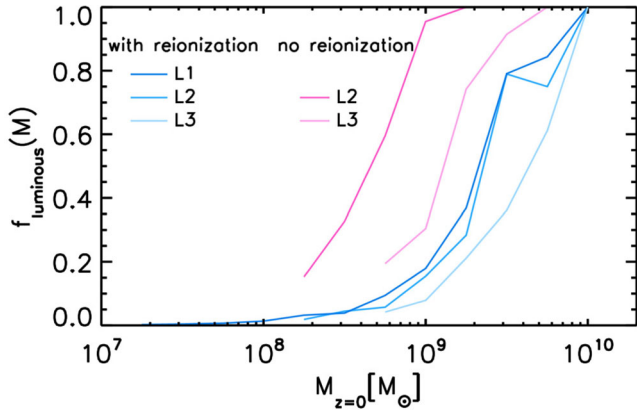
Figure 2. Fraction of haloes which are luminous at $z = 0$ as a function of halo mass in simulations with and without reionization for different resolutions. When reionization is included, the fraction of luminous haloes as a function of mass is much reduced. In the simulation with reionization, the luminous fraction is converged at L2. By contrast, without reionization, the luminous fraction is not numerically converged, and would increase further with higher resolution.
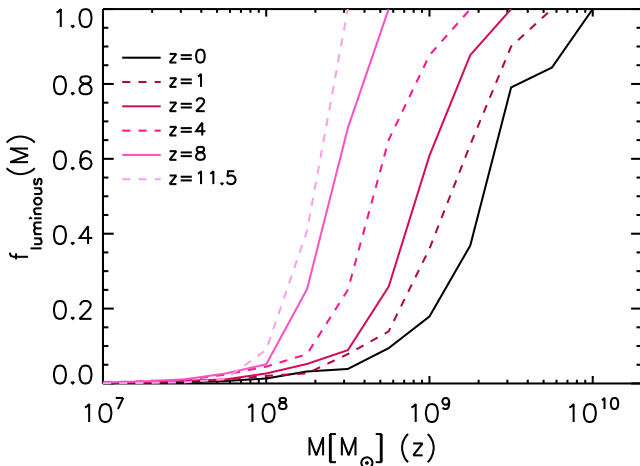
Figure 3. Fraction of haloes which are luminous as a function of halo mass at different redshifts from $z = 11.5$ to 0 in the simulation with reionization at resolution L1. At any redshift, the fraction of luminous haloes of mass below $10^8 \, \mathrm{M_\odot}$ is less than 10 per cent, and almost no haloes below $10^{7.5} \, \mathrm{M_\odot}$ contain stars. The mass scale that separates luminous from dark haloes evolves from $\sim 3 \times 10^8 \, \mathrm{M_\odot}$ at $z = 11.5$ to $\sim 3 \times 10^9 \, \mathrm{M_\odot}$ at $z = 0$.

of tidal stripping and mass-loss, leading to a decrease in average mass towards $z = 0$. By comparison, the mass of present-day field haloes is typically maximal at $z = 0$. However, as can be seen in the top-left panel, despite their present isolation, the least massive luminous field haloes in the hydrodynamic simulation also achieved their peak mass at $z > 0$, and have since lost mass as a result of tidal interactions. Because such orbits require an unusual combination of parameters unlikely to be found for both objects in a pair of haloes matched across the DMO and hydrodynamic simulation, this behaviour is only seen directly in the hydrodynamic simulation, but not among the isolated haloes of the DMO simulation which have luminous counterparts.

While such 'escaped' satellites account for only a small fraction of all presently isolated haloes, star formation in haloes with peak mass below $10^9 \, \mathrm{M_\odot}$ is also very rare. Consequently, among the small number of isolated galaxies in such low-mass haloes, the

probability of having had such an exceptional history is significantly increased.

In this context, it is also worth noting that Teyssier, Johnston & Kuhlen (2012) have computed the probability that haloes of isolated dwarf galaxies within the Local Group are 'escaped' satellites, based on orbits of haloes measured in the Via Lactea II DMO simulation. They found that ~ 13 per cent of haloes within 1.5 Mpc have passed through the Milky Way's virial radius. While our simulation volume at L1 contains only six luminous isolated haloes of $10^{8.5}$–$10^9 \, \mathrm{M_\odot}$, their assembly histories suggest that for field dwarf galaxies in very low-mass haloes, the probability of past tidal interactions is significantly higher than for typical isolated haloes in this mass range, ~ 99 per cent of which are non-luminous.

4.2 Star formation

While low-mass haloes have to assemble their mass early on in order to survive reionization, star formation itself begins later in many haloes. Of all haloes that contain galaxies at $z = 0$ in our simulation at resolution L1 including reionization, ~ 8 per cent have started forming stars before $z = 11.5$, with a median redshift of $z = 6$ for the first stars to form in each galaxy.

Observed dwarf spheroidal galaxies are known to have predominantly old stellar populations (e.g. Weisz et al. 2014a), and in particular, most ultrafaint dwarf galaxies are consistent with having formed the majority of their stars before $z = 6$, (or more than 12.8 Gyr ago) (Brown et al. 2014; Weisz et al. 2014b). In Fig. 5, we show the redshift of first star formation and the stellar-mass-weighted median formation redshift of all stars in each galaxy, as a function of present-day stellar mass (left-hand panel), and present-day halo mass (right-hand panel). Satellite and field haloes can be identified on both panels.

Some of the oldest stars which formed before reionization can be found in haloes of nearly all masses today. By contrast, the median star formation redshift depends more strongly on galaxy and halo mass. While more massive galaxies ($M_\star > 10^8$, $M_{200} > 10^{10} \, \mathrm{M_\odot}$) typically have median star formation redshifts of $z \sim 0.7$ (or median stellar ages younger than ~ 6.5 Gyr), most lower mass galaxies contain older stellar populations. In particular, most satellite galaxies with stellar masses of less than $10^6 \, \mathrm{M_\odot}$ and halo masses of only a few times $10^8 \, \mathrm{M_\odot}$ formed the bulk of their stars before $z = 4$, and have median stellar ages in excess of 12 Gyr. In our simulations, these very low mass but luminous haloes are predominantly stripped satellites, reminiscent of the observed faint satellites of the MW.
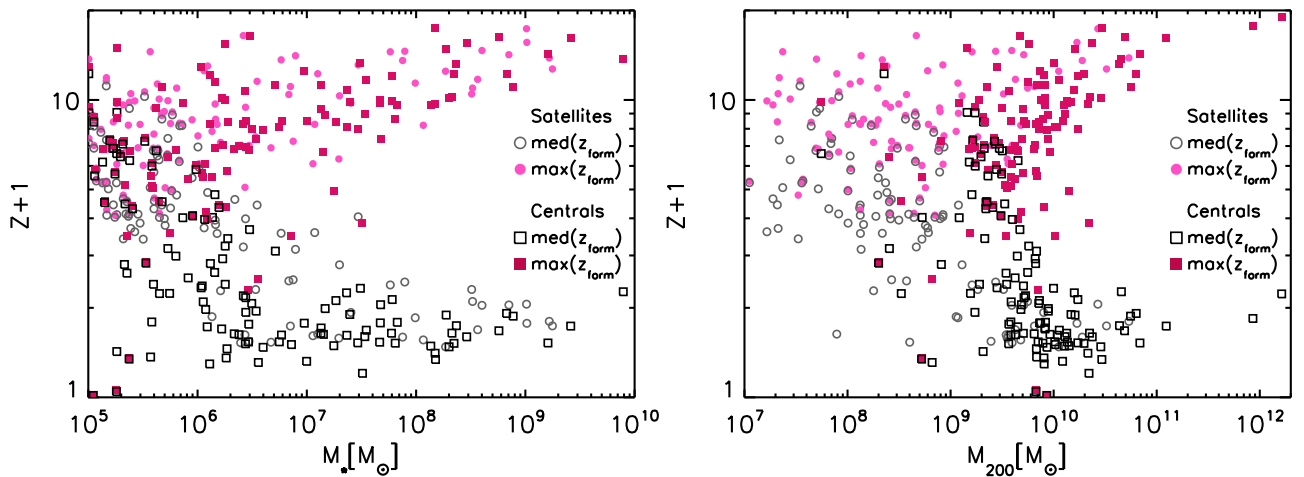
4.3 Halo formation redshifts

The difference in assembly history between luminous and non-luminous haloes can also be expressed as a bias in formation redshift, $z_{1/2}$, defined as the redshift at which a halo's most massive progenitor first reaches 1/2 of its peak mass. In Fig. 6, we plot the formation redshifts of luminous and non-luminous haloes as a function of their peak mass.

While the total population of haloes shows only a weak dependence of formation redshift on mass (in agreement with Fakhouri, Ma & Boylan-Kolchin 2010), the subpopulations of luminous and non-luminous haloes *both* show a strong mass dependence, with lower mass haloes forming earlier. This result can be understood because at any mass, luminous haloes form earlier than dark haloes: haloes of low mass have to form earlier to be luminous, and haloes of high mass have to form later to be dark. The increase in the fraction of luminous haloes with mass then offsets the negative
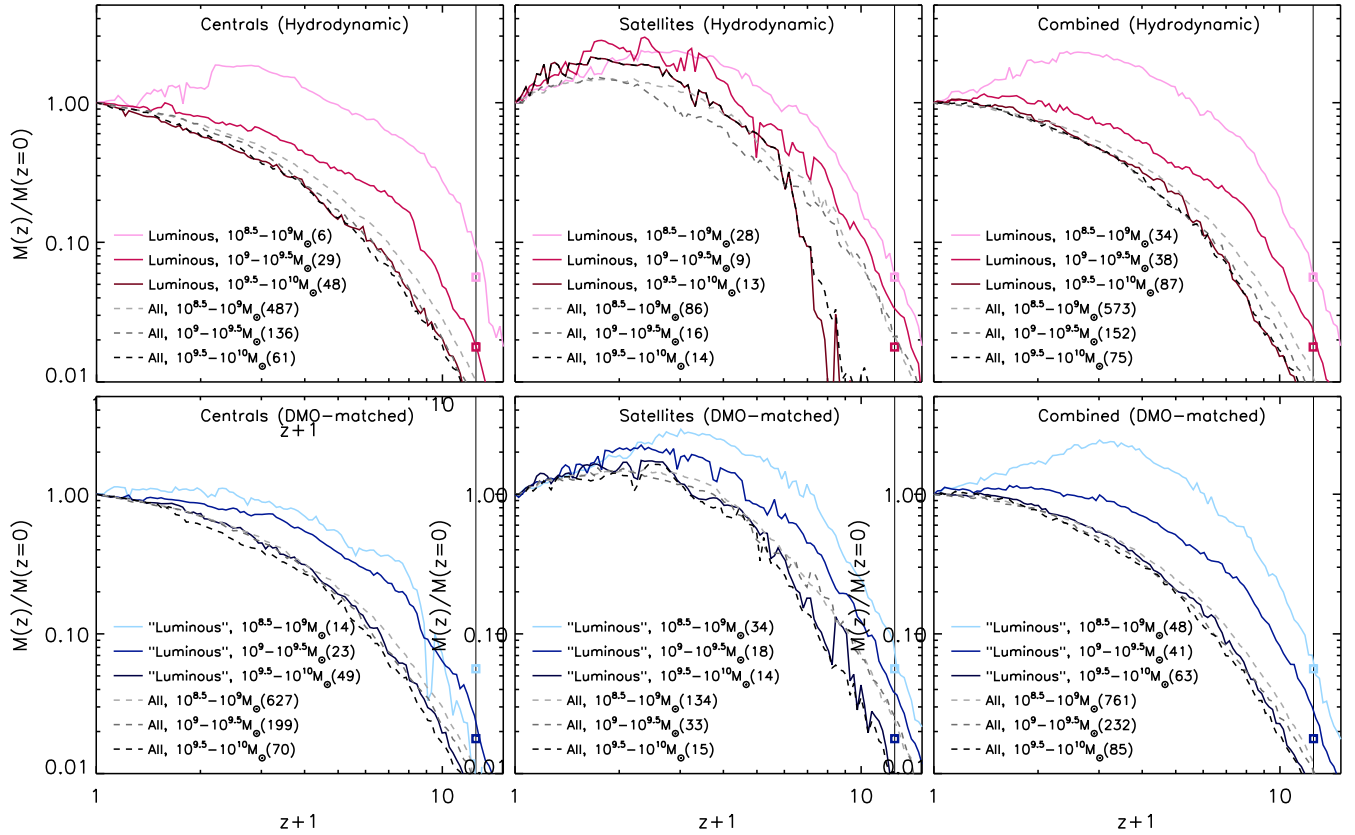
Figure 4. Mass assembly history for present-day field haloes (left), present-day satellites (centre) and the combination of both (right). Haloes are grouped according to mass at $z = 0$, as measured in the hydrodynamic simulation (top row), and as measured in the DMO simulation (bottom row), at resolution L1. The number of objects in each subset is given in brackets. The vertical lines indicate $z = 11.5$, the time of hydrogen reionization, and the squares indicate mass ratios that corresponds to the same halo mass ($10^{7.5}$ $M_\odot$) at this time for each final mass bin. As indicated by the dashed lines, haloes of lower final mass generally formed earlier, but this trend is greatly amplified for luminous haloes. With decreasing final mass, luminous haloes become increasingly biased towards earlier formation times. Tidal stripping typically results in mass-loss for satellites, whereas field haloes tend to reach their peak mas at $z = 0$. However, note that luminous field haloes with masses below 10^9 $M_\odot$ today are also likely to have been tidally stripped in the past, leading to an evolution more similar to that of satellites.

Figure 5. Redshift of first star formation (filled symbols) and stellar-mass weighted median star formation redshift (open symbols) of individual central (squares) and satellite (circles) galaxies, as a function of stellar mass (left-hand panel) and halo mass (right-hand panel) at $z = 0$, in the simulation at resolution L1 including reionization. Haloes across the mass range begain star formation before reionization at $z = 11.5$, and pre-reionization stars are today found in haloes of all different masses. As the halo mass and stellar mass decreases, stellar populations are increasingly older. In particular, dwarf galaxies in haloes of $<10^8$ $M_\odot$, most of which are satellites, typically have median star formation redshifts of $z > 4$ and median stellar ages in excess of 12 Gyr.
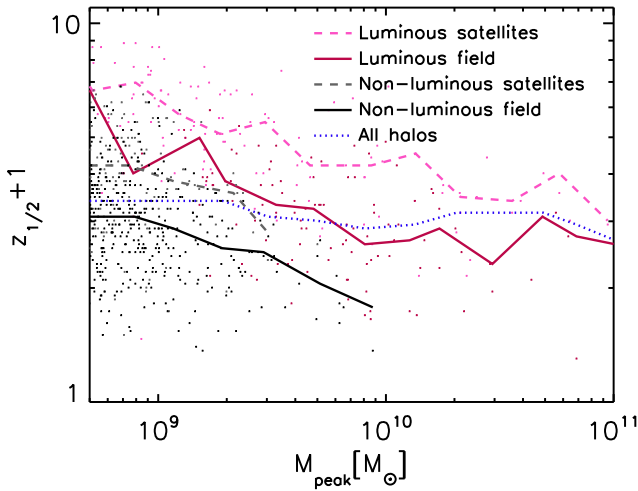
Figure 6. Redshift when a halo reached half of its peak mass as a function of peak mass in the simulation at resolution L1. Luminous haloes which were able to cool stars in the presence of reionization formed significantly earlier than non-luminous ones of the same peak mass. As the required evolution bias increases for lower mass haloes, both luminous and dark haloes show a strong mass evolution of the formation redshift, whereas the total halo population does not.

correlation of mass with formation redshift in each subset to give a total population in which mass and formation time are largely uncorrelated.

The average formation redshift of present-day satellites is higher than that of present-day field haloes. Satellite haloes typically reach their peak mass at $z_{\rm infall}$ before $z = 0$, while the masses of field haloes typically continue to increase to $z = 0$. The exception are present-day field haloes that experienced past tidal interactions, which, like satellites, are below their peak mass today. As noted in Section 4.1, among field haloes with peak masses below $10^9 \, {\rm M}_\odot$ that are luminous the probability of such a history is increased significantly.

In summary, we find that the progenitors of present-day dwarf galaxies do not have the assembly histories typical of dark matter haloes of their mass or $v_{\rm max}$. While dark haloes of peak mass $10^9 \, {\rm M}_\odot$ form at $z_{1/2} \sim 2$, haloes of the same mass that host galaxies have a formation redshift of $z_{1/2} \sim 3$–4.

4.4 Velocity–mass relation

Haloes that formed earlier have higher concentration, and therefore higher maximum circular velocity, $v_{\rm max}$, for a given mass. In addition, more concentrated haloes can cool gas more efficiently, limiting the photoevaporating effect of reionization. Since both early mass growth and the resistance to photoevaporation enhance the probability for star formation, we expect low-mass galaxies to be hosted preferentially by haloes of higher $v_{\rm max}$–mass ratios.

In Fig. 7 we show the relation between $v_{\rm max}$ and halo mass, either evaluated at $z = 0$ or at $z_{\rm peak}$, the time of peak mass. While the total population follows the $v_{\rm max}$–mass relations expected for ΛCDM (e.g. Klypin, Trujillo-Gomez & Primack 2011, not shown), we find that below $10^{9.5} \, {\rm M}_\odot$, luminous haloes have significantly higher $v_{\rm max}$–mass ratios than non-luminous ones. As the fraction of luminous haloes in our hydrodynamic simulation decreases with decreasing halo mass, the bias of the remaining luminous haloes increases. Similarly, at high masses where most haloes are luminous,

the remaining dark haloes are increasingly biased towards lower $v_{\rm max}$–mass ratios.

We find similar trends when we consider the haloes of the DMO simulation that are matched to luminous and non-luminous haloes. Like the luminous haloes themselves, their counterparts in the DMO simulation have much higher $v_{\rm max}$–mass ratios than the DMO counterparts of the non-luminous haloes. This confirms that the increased $v_{\rm max}$ of luminous haloes in the hydrodynamic simulation is largely explained by the fact that more concentrated haloes are intrinsically more likely to form stars.

We can examine the additional effect of baryons by directly comparing the $v_{\rm max}$–mass relation between haloes in the hydrodynamic simulation and their respective DMO counterparts. From the left-hand panel of Fig. 7, it can be seen that at peak mass, the non-luminous haloes and their DMO counterparts follow very similar relations, while the luminous haloes in the hydrodynamic simulation are more concentrated than their DMO counterparts. This indicates that processes like gas cooling, which are stronger in the luminous than in the the non-luminous haloes, can also lead to an increase in the $v_{\rm max}$–mass ratios, an effect obviously not present in the DMO simulation.

When the two simulations are compared at $z = 0$, as is the case in the right-hand panel of Fig. 7, luminous and non-luminous haloes alike have lower average $v_{\rm max}$–mass ratios than their respective counterparts in the DMO simulation. However, this difference is small compared to the offset between luminous and dark haloes or the corresponding matched objects.

It can also be seen that satellites follow a different $v_{\rm max}$–mass relation compared to field haloes, with a lower mass for a given $v_{\rm max}$. This well-known result can be attributed to the fact that tidal stripping first removes material from the outside of an infalling halo, beyond $r_{\rm max}$, with a greater impact on halo mass than on $v_{\rm max}$. However, we also find that the difference between satellite and field haloes is strongly amplified among luminous haloes because, as we will discuss in Section 5.1, luminous and dark satellites follow significantly different orbits.

In summary, we find that luminous low-mass haloes have much higher $v_{\rm max}$–mass ratios than average haloes. This difference increases as the fraction of luminous haloes decreases towards lower masses, and is higher for satellites than for field haloes. Since we find similar trends between the respective matched haloes in DMO simulation, we attribute them mostly to the increased likelihood for star formation in more concentrated haloes, rather than to an increase of concentration due to cooling and star formation.

5 LATE-TIME EVOLUTION

In addition to the effects of assembly history and the properties of haloes directly related to reionization, the late-time evolution also influences the probability for haloes of a given mass or $v_{\rm max}$ observed *today* to host galaxies, not because it has any direct influence on star formation, but to the extent that it changes the observed halo properties relative to those that determined star formation in the early universe. Since the late-time evolution depends on environment, this affects the relative spatial distributions of luminous and dark haloes within the Local Group.

In the previous section, we showed that the progenitors of luminous haloes formed significantly earlier than those of dark haloes. We also noted clear differences between the evolution of satellites and centrals. In this section, we examine the late-time effects in more detail, and show in particular how tidal stripping and the fact that satellites stop growing after infall, can introduce a strong
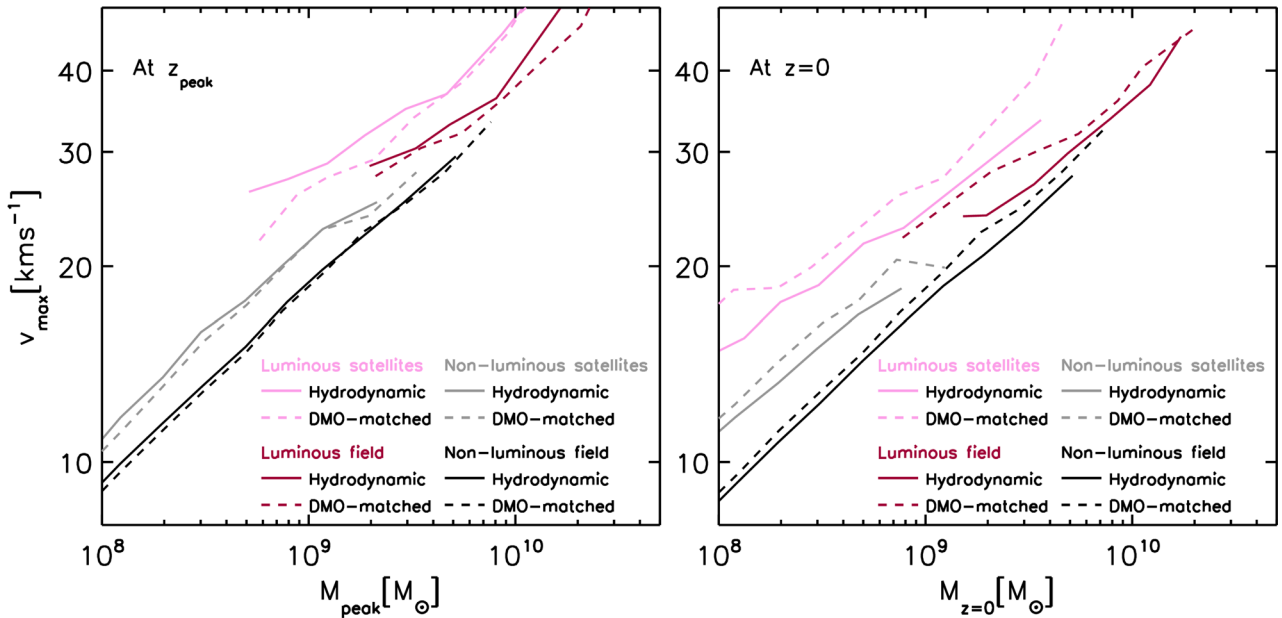
Figure 7. The relation between halo mass and v_{max} at the time of peak mass (left-hand panel) and at $z = 0$ (right-hand panel) from the simulation at resolution L1 including reionization. Since stars form preferentially in haloes of high concentration, luminous haloes are on average more concentrated than dark haloes. The effect of galaxy formation itself on the halo is manifest in the difference between the relations measured in the hydrodynamic simulation and those measured from the matched DMO simulation. At peak mass, luminous haloes in the hydrodynamic simulation have higher v_{max}/mass ratios than their DMO counterparts, indicating that gas cooling leads to an increase in concentration. At $z = 0$ haloes of all type are typically less concentrated in the hydrodynamic simulation than in the DMO simulation.
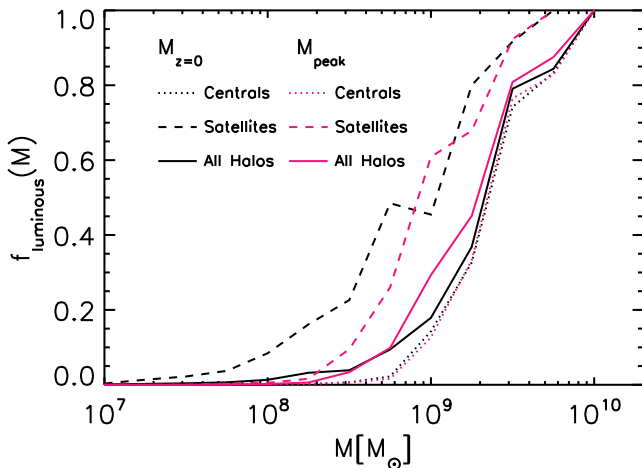
Figure 8. Fraction of central (dotted lines), satellite (dashed lines) and all haloes (solid lines) which are luminous at $z = 0$ in the simulation at L1 with reionization included, as a function of $z = 0$ mass (black), and as a function of peak halo mass (magenta). Most centrals reach their peak mass at $z = 0$, so the relation is nearly identical to that at z_{peak}. The mass scale separating luminous and non-luminous haloes is lower for centrals, and there is a noticeable evolution below 10^9 M$_\odot$, where the fraction of luminous satellites at $z = 0$ is significantly higher than for the same halo mass at z_{peak}.

environmental dependence on the relation between observable galaxies and the underlying halo population.

In Fig. 8 we compare the fraction of luminous satellite haloes and central haloes, both as a function of present-day mass, and as a function of peak halo mass, for the simulation at resolution L1

including reionization. For centrals, which are typically at their peak mass at $z = 0$, the luminous fraction expressed in terms of either present-day or peak halo mass is nearly identical. For satellites, for which a given halo mass today corresponds to a higher peak halo mass than for centrals (cf. Section 4.1), the luminous fraction for a given halo mass is higher than for centrals.

The difference in the luminous fraction between centrals and satellites can be seen both at z_{peak} (due to the fact that centrals continue to grow after the time when the corresponding satellite's halo mass has already peaked), and is even stronger at $z = 0$, where stripping of satellites typically leads to a reduction in halo mass below its peak value. Both the difference in the luminous fraction between centrals and satellites, and the difference between the luminous fractions of satellites measured at z_{peak} and measured at $z = 0$ increase as the overall luminous fraction decreases towards lower halo masses.

Because most haloes of a given mass are centrals, the luminous fraction of all haloes closely follows that of central haloes, and is similar at $z = 0$ and z_{peak}. However, due to the much larger luminous fraction of low-mass ($<10^9$ M$_\odot$) satellites compared to low-mass centrals, most low-mass *luminous* haloes (and hence most galaxies in low-mass haloes in our LG simulations) are satellites.

5.1 Satellite evolution

The evolution of satellite haloes is driven by tidal effects, which further separate their present-day properties from those of their progenitors. Among satellite haloes of the same mass or v_{max} to-day, those that experienced greater mass-loss had more massive progenitors prior to infall, and therefore a higher probability for star formation. This introduces additional biases between dark and luminous satellites that depend on their infall times and orbital parameters.
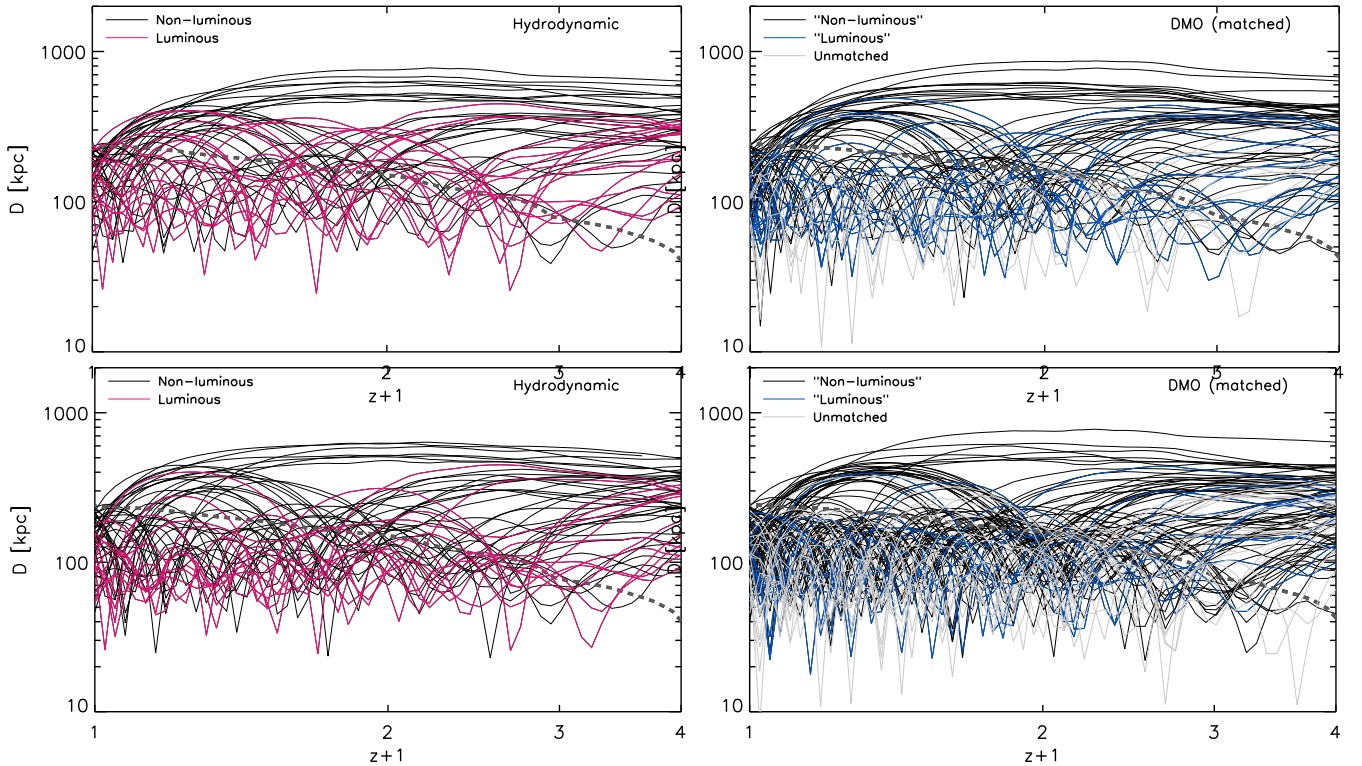
Figure 9. Evolution of galactocentric distance for dark and luminous satellites of the simulated 'Milky Way', as identified directly in the hydrodynamic simulation (left column), or as matched from the DMO simulation (right column) at resolution L1. Satellite haloes are selected by present-day mass in the range 10^8–10^9 $M_\odot$ (top row) or present v_{max} in the range 12–20 $km\,s^{-1}$ (bottom row). In each panel, the grey dashed line shows the evolution of the host halo's virial radius, r_{200}, in both simulations. Within this range of mass or v_{max}, the orbits of luminous and dark haloes differ significantly. Also note the lower number of objects in the hydrodynamic simulation compared to the DMO simulation, due to the reduction of v_{max} and mass of individual haloes by baryonic effects.

In Fig. 9 we compare the orbits of luminous and dark low-mass satellites of one of our simulated Milky Way like haloes. We identify satellites as self-bound haloes within the virial radius of the host at $z = 0$, r_{200}, defined as the radius within which the mean density is $200\times$ the *critical* density, and define the infall redshift, z_{infall}, as the redshift when a satellite first crosses r_{200}. Selecting satellites either by their present mass or present v_{max}, it can be seen that the orbits of luminous haloes in the mass range of 10^8–10^9 $M_\odot$ or the v_{max} range of 12–20 $km\,s^{-1}$ differ significantly from those of dark haloes of the same present mass: they fall in earlier and come closer to the centre of the host.

We note that the same effect can be seen between the haloes of the DMO simulation which are matched to luminous and dark haloes in the hydrodynamic simulation and shown in the right column of Fig. 9. The matching of low-mass satellites is imperfect because satellites can evolve differently in the two simulations. Nevertheless, it underlines the fact that the different orbits of luminous and non-luminous satellites are primarily caused by a selection effect of the progenitors imposed by reionization, and not by differences in the baryonic components between the luminous and dark satellites. However, the overall number of satellites is reduced in the hydrodynamic simulation due to the loss of baryons, consistent with the results of Sawala et al. (2013).

The top panel of Fig. 10 shows the distribution of infall redshifts of luminous and non-luminous satellites in the v_{max} range of 12–20 $km\,s^{-1}$, compatible with the haloes of Milky Way dwarf spheroidal satellites inferred from stellar kinematics (Walker et al.

2007). These results include satellites of all 24 M31 and Milky Way like haloes in our 12 Local Group simulations at resolution L2. Luminous satellites in this v_{max} range were accreted significantly earlier, with a median infall redshift of 1.55 ± 0.05, compared to 1.00 ± 0.06 for non-luminous satellites.

It is worth noting that in addition to *mass-loss* through tidal stripping, the infall of a satellite also marks the end of *mass growth* that a field halo would typically experience. For the same infall mass, an earlier infall time corresponds to a higher mass in the early universe, further enhancing the probability of star formation.

In the middle and bottom panels of Fig. 10, we compare the same population of satellites described above in terms of the ratio between the infall velocity of the satellite and the virial velocity of the host halo at the time of infall, v/v_{200}, and in terms of the ratio between the radial component and the total infall velocity, v_r/v. Again, we find that luminous satellites in this v_{max}-range fell in with higher infall velocities and on more radial orbits, both of which made them more susceptible to tidal stripping. The median ratio between the infall velocity and the halo v_{200} is $v/v_{200} = 1.32^{+0.08}_{-0.06}$ for luminous satellites, and $v/v_{200} = 1.23^{+0.02}_{-0.03}$ for non-luminous satellite haloes in this v_{max}-range. For the same two sets of objects, the median ratio between the radial component and the total infall velocity is $v_r/v = 0.79^{+0.06}_{-0.04}$ for luminous satellites and $v_r/v = 0.71^{+0.02}_{-0.02}$ for dark ones, where the errors indicate the 68 per cent confidence range in each case.

The post-infall changes in mass and v_{max} among luminous and dark satellites as functions of present mass and v_{max} are compared
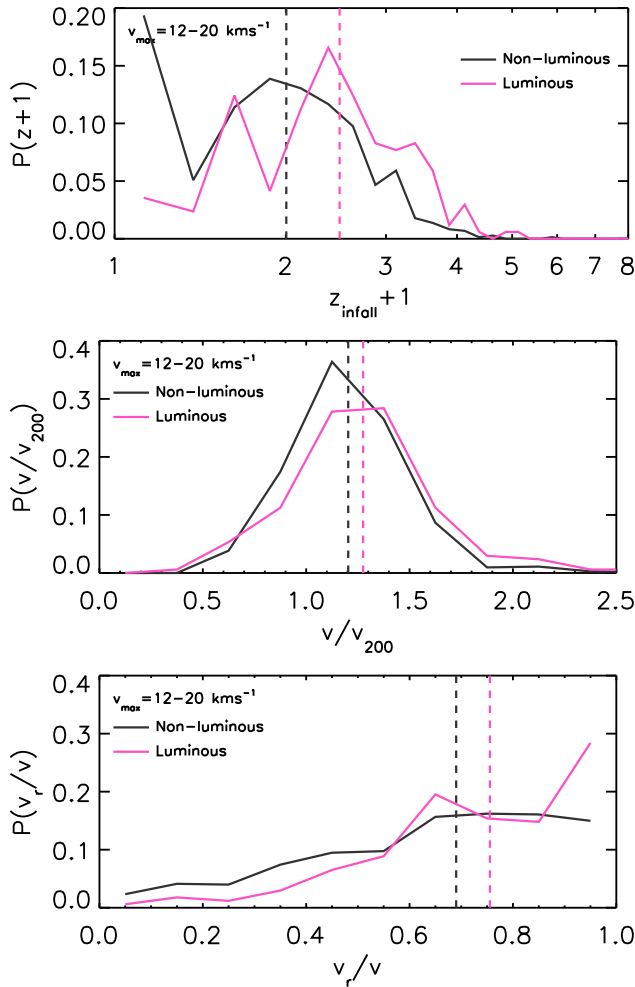
Figure 10. Top panel: distribution of infall redshifts of luminous and non-luminous satellites in the present-day v_{max} range of 12–20 km s^{-1}, from 12 volumes at resolution L2. Middle panel: distributions of infall velocities of satellites in the divided by v_{200} of the host halo at the time of infall. Bottom panel: distributions of the ratio between the radial component and the total infall velocity. Dashed lines indicate the median values on all panels. Luminous haloes in this v_{max} range fell in significantly earlier, with higher velocities and on more radial orbits compared to non-luminous haloes.

in Fig. 11. As expected, luminous satellites of low present mass are increasingly more likely to have lost mass due to stripping. Whereas dark satellites have typically lost only 1/3 of their mass after infall, independent of present mass, luminous satellites of 10^9 M$_\odot$ have lost of 1/2 of their mass in the median, a fraction that increases further for lower mass haloes. While dark satellites have typically reduced their v_{max} by less than 10 per cent, luminous satellites of 20 km s^{-1} today have typically experienced a reduction in v_{max} by 25 per cent.

The bias seen in the infall times, orbits, and reduction in mass and v_{max} of satellites similar to those that host the observed dwarf spheroidal galaxies may change previous assumptions about their evolution: whereas Peñarrubia, McConnachie & Navarro (2008) have shown using DMO simulations that the v_{max} of most dwarf-sized *haloes* should not be affected by tidal effects, our simulations show that the opposite is be true for the subset of haloes that actually host the dwarf spheroidal *galaxies*. Those satellite galaxies that today inhabit haloes of $v_{max} \sim 20$ km s^{-1} typically formed in haloes of ~ 30 km s^{-1}.
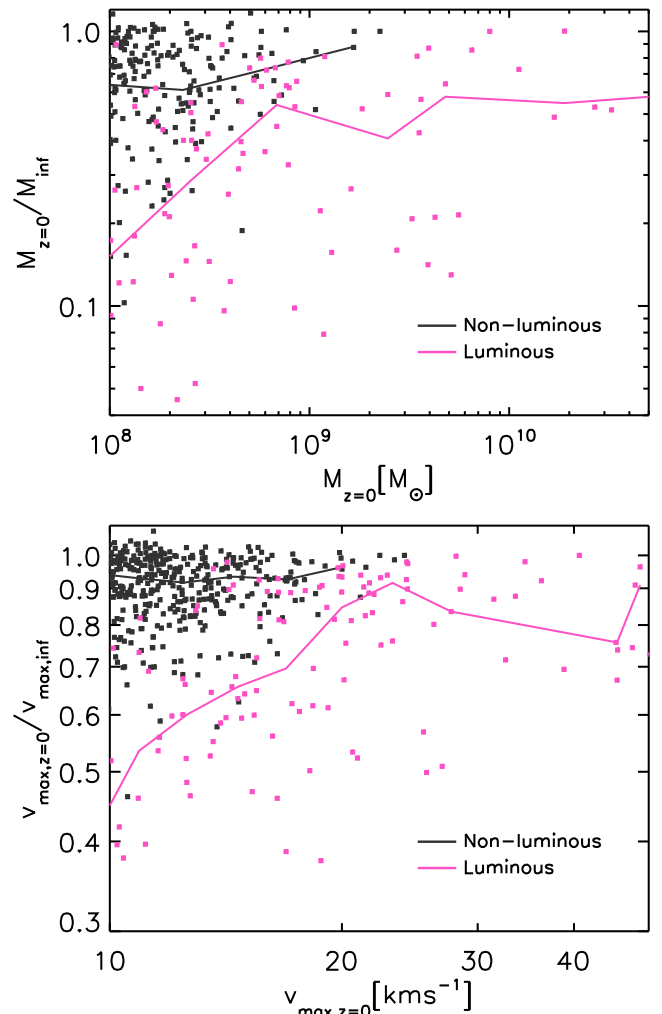
Figure 11. Change in mass relative to mass at z_{infall} as a function of present mass (top panel), and change in v_{max} relative to v_{max} at z_{infall} as a function of present v_{max} (bottom panel), for luminous and non-luminous satellite haloes of the parent halo shown in Fig. 9, at resolution L1. Lines indicate the median values. As haloes with infall masses $<10^{9.5}$ M$_\odot$ or $v_{max} < 25$ km s^{-1} are unlikely to host galaxies, luminous haloes with such lower present values are likely to have experienced a much more significant decrease in mass and v_{max} from their peak values compared to non-luminous haloes.

5.2 Dwarf galaxies and haloes in the Local Group

The effect of stripping that separates the luminous and non-luminous satellites also extends to a marked difference between satellite and field haloes within the Local Group, and differences in the distribution of luminous and dark haloes beyond the virial radius of its two main galaxies.

In Fig. 12 we show the fraction of haloes of a given mass or v_{max} today that are populated by galaxies, as a function of distance to the Milky Way-like galaxy. It can be seen that while all satellites with $M > 10^9$ M$_\odot$ or $v_{max} > 20$ km s^{-1}, as well as a large fraction of lower mass haloes, are populated inside 200 kpc, the fraction decreases with increasing distance (an increase at $\sim$800 kpc can be attributed to the satellites of the second massive halo in the simulated Local Group, i.e. the halo of 'M31').

The locations of individual luminous and non-luminous haloes above 10^7 M$_\odot$ at $z = 0$ within one of our Local Group simulations can be seen in Fig. 13. The top and bottom panels show the positions
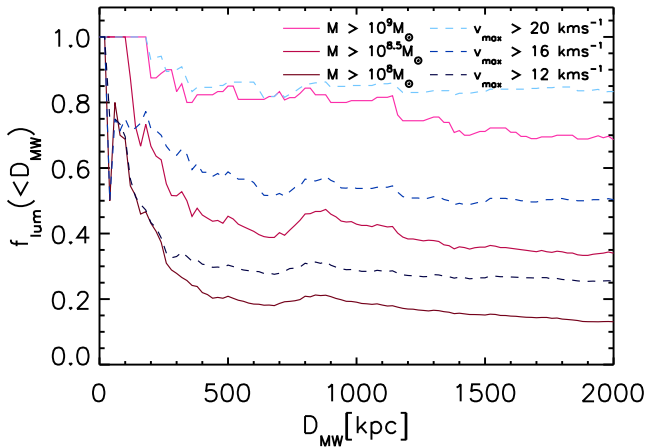
Figure 12. Fraction of luminous haloes above a given mass (solid lines) or v_{max} (dashed lines), within a given distance from the centre of the simulated 'Milky Way', in the simulation at resolution L1. At fixed mass, haloes within ~300 kpc of the Milky Way are much more likely to contain galaxies than more isolated haloes, and the environmental dependence is stronger among haloes of lower present mass or v_{max}.

of haloes and the projected dark matter density within 2 Mpc to the centre of the Local Group, and within 400 kpc of one of the Milky Way like haloes, respectively. Low-mass luminous haloes are predominantly found close to the larger galaxies, where stripping has lead to a significant reduction in mass, and where the mass growth has been truncated by infall compared to more isolated haloes.

While ram pressure stripping can quench star formation and introduce environmental dependencies on the properties of low-mass galaxies, gas is not responsible for the environmental dependence of the luminous fraction. It is primarily driven by the fact that, as a result of tidal stripping, haloes of a given mass or v_{max} today that are closer to the central galaxies typically had higher masses or v_{max} in the early universe, and therefore a higher probability for star formation.

This result implies that there are fewer isolated dwarf galaxies in the Local Group than a simple extrapolation based on v_{max} or mass from the Milky Way and M31 satellites would suggest.

6 DISCUSSION AND SUMMARY

We have analysed a set of hydrodynamic and DMO simulations of the Local Group in order to study how galaxies populate low-mass haloes in the presence of reionization. We have shown that reionization greatly reduces the number of dwarf galaxies that form, and that even at fixed mass or v_{max} today, the subset of haloes that host the majority of the Local Group's dwarf galaxies differ significantly from the total halo population.

The differences between the luminous and non-luminous haloes result from a combination of early-time and late-time effects. Haloes of mass below ~$3 \times 10^9 \, M_{\odot}$ or v_{max} below ~25 km s^{-1}, which in our simulations host dwarf galaxies up to ~$10^7 \, M_{\odot}$, comparable in stellar mass to the MW dwarf spheroidals, assembled their mass significantly earlier than typical dark matter haloes of the same present-day mass or v_{max}. Since haloes that form earlier are more concentrated, and also because more concentrated haloes are more resistant to photoevaporation, those haloes that contain stars have significantly higher v_{max}–mass ratios.

The late-time evolution of haloes, and in particular tidal stripping, introduces further biases between the luminous and non-luminous haloes. Unlike the selection effects which operate in the early universe, these effects do not determine which haloes are able to form stars, but they affect the relation between those halo properties that either allowed or prevented star formation, and the present-day properties of luminous and non-luminous haloes in the Local Group environment. We find that the haloes of satellite galaxies with mass and v_{max} values similar to those of the observed dwarf spheroidals experienced much stronger tidal stripping than comparable non-luminous satellites. The Milky Way or M31 satellite galaxies typically formed in haloes that were more than twice as massive and had significantly higher v_{max} values prior to infall. They also had earlier infall redshifts, higher infall velocities, and followed more radial orbits than typical dark matter haloes.

Within the Local Group, isolated haloes are much less likely to host galaxies than satellites of comparable mass or v_{max} today. In particular, present-day field dwarf galaxies that share the characteristics of dwarf spheroidals are more likely to be 'escaped' satellites than was assumed from earlier DMO studies.

The biases between the luminous and non-luminous haloes described here have to be taken into account whenever the properties of haloes or of the underlying cosmology are to be measured, but only those haloes that contain galaxies can be observed.
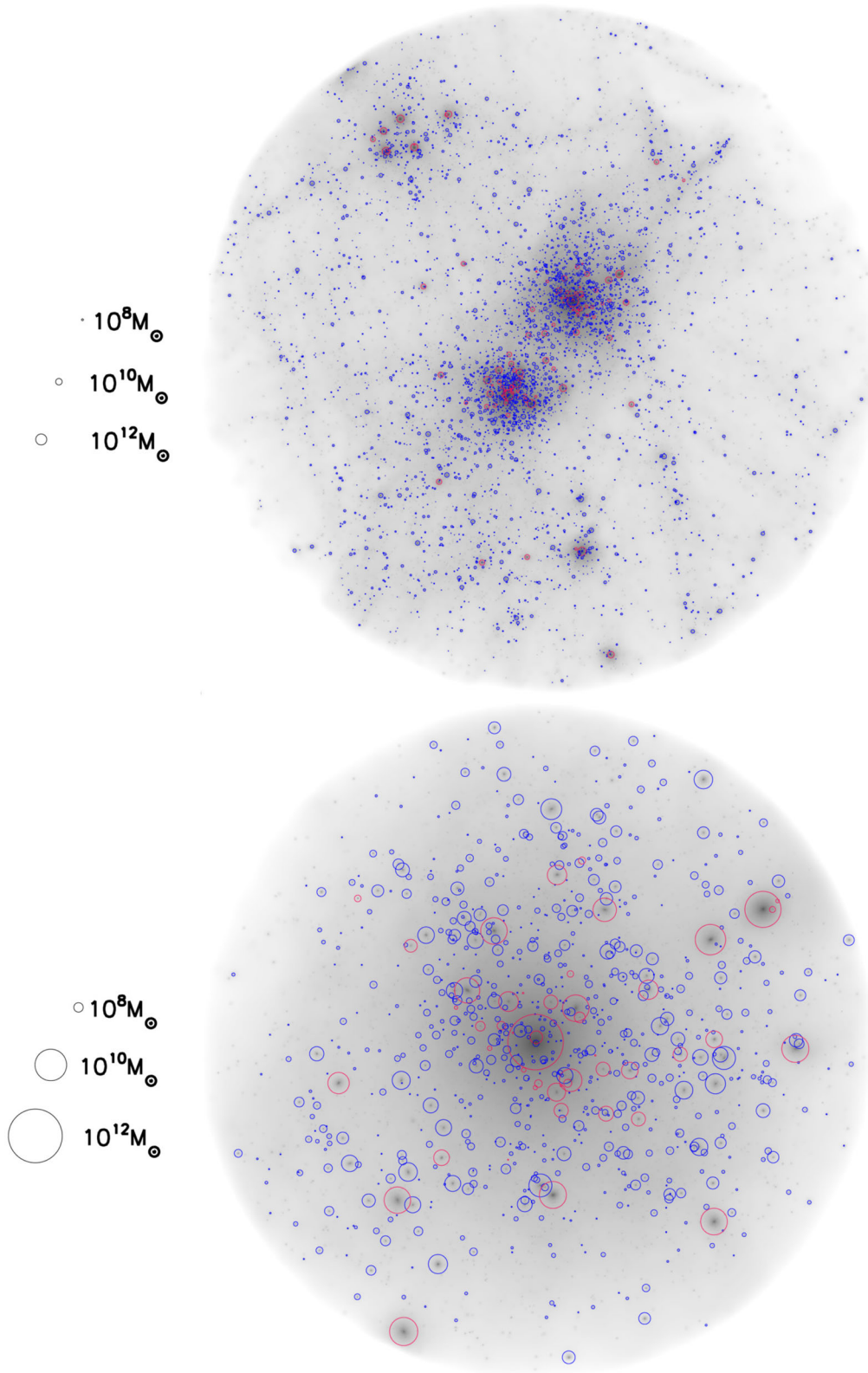
It is worth noting that our simulations still have several limitations. Our simulations assume reionization at $z = 11.5$, and while it is likely that any model which does not result in an overabundance of dwarf galaxies would yield qualitatively similar results, it is also likely that later reionization would raise the mass scales relevant for differences between luminous and non-luminous haloes, while earlier reionization would lower them. The simulations also assume that reionization is uniform and do not account for local sources of ionization. Radiative transfer is not included, cooling rates are computed in the optically thin limit, star formation is modelled in a stochastic way, and we did not include star formation in mini haloes powered by H_2 cooling. While we have shown that the fraction of haloes populated by galaxies is numerically converged, it may still depend on model parameters.

With these limitations in mind, we would like to emphasize the importance of the connection between the observable dwarf galaxies and the underlying population of dark matter haloes. As noted in the beginning, the Local Group dwarf galaxies provide the best window for studying the nature of dark matter on small scales. However, our results suggest that because reionization leaves most haloes empty, most Local Group dwarf galaxies today *typically* live in haloes that are highly *atypical*.

Figure 13. Projected density distribution of dark matter and positions of haloes at $z = 0$ in the same simulated Local Group volume including reionization at resolution L2 shown in Fig. 1, inside a sphere of radius 2 Mpc centred on the LG barycentre (top panel), and a sphere of 400 kpc radius centred on the simulated Milky Way (bottom panel). Blue and red circles indicate the positions of dark and luminous haloes above $10^7 \, M_{\odot}$, respectively, with diameter proportional to the logarithm of the mass. It can be seen that luminous haloes of low mass cluster near the two main haloes. Also, while more massive haloes are more likely to be luminous, there is no sharp mass threshold separating luminous and dark haloes at $z = 0$, since the probability of hosting a galaxy is a function of mass, assembly history, and environment.

REFERENCES

Abel T., Haehnelt M. G., 1999, ApJ, 520, L13
Benson A. J., Frenk C. S., Lacey C. G., Baugh C. M., Cole S., 2002, MNRAS, 333, 177
Booth C. M., Schaye J., 2009, MNRAS, 398, 53
Brown T. M. et al., 2014, ApJ, 796, 91
Bullock J. S., Kravtsov A. V., Weinberg D. H., 2000, ApJ, 539, 517
Crain R. A. et al., 2015, MNRAS, 450, 1937
Dalla Vecchia C., Schaye J., 2012, MNRAS, 426, 140
Davis M., Efstathiou G., Frenk C. S., White S. D. M., 1985, ApJ, 292, 371
Dolag K., Borgani S., Murante G., Springel V., 2009, MNRAS, 399, 497
Efstathiou G., 1992, MNRAS, 256, 43
Fakhouri O., Ma C.-P., Boylan-Kolchin M., 2010, MNRAS, 406, 2267
Fattahi A. et al., 2015, preprint (arXiv:1507.03643)
Haardt F., Madau P., 2001, in Neumann D. M., Tran J. T. V., eds, Clusters of Galaxies and the High Redshift Universe Observed in X-rays, CEA, Saclay, p. 64
Helly J. C., Cole S., Frenk C. S., Baugh C. M., Benson A., Lacey C., 2003, MNRAS, 338, 903
Hopkins P. F., 2013, MNRAS, 428, 2840
Jenkins A., 2010, MNRAS, 403, 1859
Jiang L., Helly J. C., Cole S., Frenk C. S., 2014, MNRAS, 440, 2115
Klypin A. A., Trujillo-Gomez S., Primack J., 2011, ApJ, 740, 102
Nickerson S., Stinson G., Couchman H. M. P., Bailin J., Wadsley J., 2011, MNRAS, 415, 257
Okamoto T., Frenk C. S., 2009, MNRAS, 399, L174
Okamoto T., Gao L., Theuns T., 2008, MNRAS, 390, 920
Pawlik A. H., Schaye J., 2009, MNRAS, 396, L46
Peñarrubia J., McConnachie A. W., Navarro J. F., 2008, ApJ, 672, 904
Planck Collaboration XVI, 2014, A&A, 571, A16
Rollinde E., Theuns T., Schaye J., Pâris I., Petitjean P., 2013, MNRAS, 428, 540
Rosas-Guevara Y. M. et al., 2015, MNRAS, 454, 1038
Sawala T., Guo Q., Scannapieco C., Jenkins A., White S., 2011, MNRAS, 413, 659
Sawala T., Frenk C. S., Crain R. A., Jenkins A., Schaye J., Theuns T., Zavala J., 2013, MNRAS, 431, 1366
Sawala T. et al., 2014, preprint (arXiv:1412.2748)
Sawala T. et al., 2015, MNRAS, 448, 2941
Schaller M., Dalla Vecchia C., Schaye J., Bower R. G., Theuns T., Crain R. A., Furlong M., McCarthy I. G., 2015, MNRAS, 454, 2277
Schaye J., 2004, ApJ, 609, 667
Schaye J., Dalla Vecchia C., 2008, MNRAS, 383, 1210
Schaye J., Theuns T., Rauch M., Efstathiou G., Sargent W. L. W., 2000, MNRAS, 318, 817
Schaye J. et al., 2015, MNRAS, 446, 521
Shen S., Madau P., Conroy C., Governato F., Mayer L., 2014, ApJ, 792, 99
Somerville R. S., 2002, ApJ, 572, L23
Springel V., 2005, MNRAS, 364, 1105
Springel V., White S. D. M., Tormen G., Kauffmann G., 2001, MNRAS, 328, 726
Springel V., Di Matteo T., Hernquist L., 2005, MNRAS, 361, 776
Teyssier M., Johnston K. V., Kuhlen M., 2012, MNRAS, 426, 1808
Theuns T., Schaye J., Zaroubi S., Kim T.-S., Tzanavaris P., Carswell B., 2002, ApJ, 567, L103
Walker M. G., Mateo M., Olszewski E. W., Gnedin O. Y., Wang X., Sen B., Woodroofe M., 2007, ApJ, 667, L53
Weisz D. R., Dolphin A. E., Skillman E. D., Holtzman J., Gilbert K. M., Dalcanton J. J., Williams B. F., 2014a, ApJ, 789, 147
Weisz D. R., Dolphin A. E., Skillman E. D., Holtzman J., Gilbert K. M., Dalcanton J. J., Williams B. F., 2014b, ApJ, 789, 148
Wiersma R. P. C., Schaye J., Smith B. D., 2009a, MNRAS, 393, 99
Wiersma R. P. C., Schaye J., Theuns T., Dalla Vecchia C., Tornatore L., 2009b, MNRAS, 399, 574

This paper has been typeset from a TEX/LATEX file prepared by the author.